



City Research Online

City, University of London Institutional Repository

Citation: Vidakovic, M., Armakolas, I., Sun, T., Carlton, J. & Grattan, K. T. V. (2016). Fibre Bragg Grating-based Acoustic Sensor Array for Improved Condition Monitoring of Marine Lifting Surfaces. *Journal of Lightwave Technology*, 34(18), pp. 4336-4342. doi: 10.1109/jlt.2016.2601122

This is the accepted version of the paper.

This version of the publication may differ from the final published version.

Permanent repository link: <https://openaccess.city.ac.uk/id/eprint/15449/>

Link to published version: <https://doi.org/10.1109/jlt.2016.2601122>

Copyright: City Research Online aims to make research outputs of City, University of London available to a wider audience. Copyright and Moral Rights remain with the author(s) and/or copyright holders. URLs from City Research Online may be freely distributed and linked to.

Reuse: Copies of full items can be used for personal research or study, educational, or not-for-profit purposes without prior permission or charge. Provided that the authors, title and full bibliographic details are credited, a hyperlink and/or URL is given for the original metadata page and the content is not changed in any way.

City Research Online:

<http://openaccess.city.ac.uk/>

publications@city.ac.uk

Fibre Bragg Grating-based Acoustic Sensor Array for Improved Condition Monitoring of Marine Lifting Surfaces

Miodrag Vidakovic, Ioannis Armakolas, Tong Sun, John Carlton and Kenneth T. V. Grattan

Abstract – This paper discusses a novel approach to monitoring marine lifting surface conditions through using arrays of Fibre Bragg Grating (FBG)-based acoustic sensors in a marine rudder. Results from these optical sensor arrays are then cross compared with those from conventional piezoelectric (PZT) sensors. A successful proof-of-concept evaluation of the optical sensor approach was, however, first undertaken by using cascaded FBGs integrated into a glass plate, monitoring the response to dropping a standard metal ball at different locations. Data obtained were compared with co-located conventional PZT sensors acoustic sensors for comparison using triangulation to determine the location of the excitation source (a sonotrode). The results obtained verify the excellent performance of the FBG-based sensors due to the excellent agreement between these different sensor types. This gives confidence to the next-stage to scale-up the FBG sensor arrays for other marine structures, with early identification of the initiation of cavitation erosion an important priority for better operational reliability and scheduling of maintenance of marine vessels.

Index Terms – Acoustic emission, cavitation, Fibre Bragg Grating (FBG) sensors, piezoelectric (PZT) sensors, structural health monitoring (SHM), source location estimation

I. INTRODUCTION

Acoustic emission (AE) detection has been widely used for the non-destructive and non-invasive structural assessment of bridges, viaducts or even masonry historical buildings [1], to determine damage location and thus predict better structural service lifetimes [2]. Crack initiation in such structures generates AE signals, at frequencies ranging from tens of kHz to hundreds of kHz, allowing the location of the AE source and the power generated to determine the scale of the cracks formed. Marine cavitation erosion degrades propellers, occurring when the ship's wake quality is inadequate and rudders, shafting support brackets and stabilization fins may also induce cavitation and with that the onset of erosion, leading to poor performance, reduced efficiency or induced structural damage [3-5]. Various civil and marine structures have metallic plate/shell and stiffeners that are subjected to corrosion and fatigue damage, where guided waves (especially Lamb waves) with particular frequencies can travel relatively long distances with low loss, offering large-area coverage [6]. The propagation

characteristics of such Lamb waves have been analyzed extensively in the literature [6-8]. Thus they are widely used in non-destructive Structural Health Monitoring (SHM) of plate structures as they are scattered and the reflected energy captured allows an estimation of the type and size of the damage encountered [9]. Here PZT based transducers are widely used due to low cost, reliability and robustness – but they show key limitations when electromagnetic Interference (EMI) is present and remote monitoring is required [10, 11, 12]. Thus they are not sufficiently versatile for measurements under more adverse circumstances, for example in remote monitoring applications where long cable lengths between the transducer and the receiver are used and EMI effects and ‘signal fade’ are seen over these over long distances. [13]. Fibre optic acoustic emission sensors offer an alternative – the majority of such sensors (hydrophones) are based on fibre optic interferometry, such as using Mach-Zehnder [14], Michelson [15] or Fabry-Parot techniques [16, 17]. Fibre Bragg Grating (FBG)-based methods are an excellent alternative for AE sensing applications [18] and recently, distributed feedback (DFB) fibre lasers have been used, as reported elsewhere [19].

Fibre Bragg Grating-based devices represent one of the most successful optical fibre sensors for industrial applications (e.g. for the measurement of strain, temperature, and a range of other parameters [20, 21]). They can readily be multiplexed, are small size and lightweight, making them well suited to multi-location, multi-parameter measurements even in hazardous or indeed extreme environments [10].

With their use as AE sensors, two main detection methods are reported [22] – using a tunable laser with its line centre at a wavelength at the 3dB position in the FBG reflection spectrum. The laser power measured [23] – carries the sensor information – but these are high cost systems, which are hard to multiplex. Optical filter demodulation, (with a narrow spectral bandwidth), uses light reflected from an FBG sensor through an optical filter, whose transmitted intensity will vary with the acoustic pressure [24-27]. This latter approach is explored and developed further in this work, focusing on sensor multiplexing and the simultaneous detection of multiple acoustic signals carrying the information, taking the work further than what has been discussed previously in the literature [28-29]. To do so, the sensor system was evaluated first by being instrumented

Miodrag Vidakovic, Ioannis Armakolas, Tong Sun, John Carlton and Kenneth T. V. Grattan are with School of Computer Sciences, Mathematics and Engineering, City University London, United Kingdom (emails: Miodrag.Vidakovic.1@city.ac.uk; Ioannis.Armakolas.1@city.ac.uk;

t.sun@city.ac.uk; john.carlton.1@city.ac.uk; K.T.V.Grattan@city.ac.uk;)
Support from the Royal Academy of Engineering and the George Daniels Educational Trust for Grattan is greatly appreciated.

onto a glass plate, allowing the detection of acoustic signals generated under known, standardized conditions – in this case by dropping a calibrated small mass (in this case a 0.2g steel ball bearing) from a known and fixed height onto a glass plate, to generate a consistent acoustic signal, comparing and validating results against a co-located PZT sensor, as a novel ‘proof of concept’ study. The aim in this is to validate a ‘real world’ application to instrument a marine lifting surface (with a cross-comparison from both types of sensors). The lifting surface was placed in a water tank and acoustically excited by a sonotrode at different locations, to accelerate cavitation-erosion and sensor data were extracted – captured by both electrical and optical fibre-based sensors. These were analyzed carefully and cross-compared, where the results showed that the location of the acoustic-emission source can be determined equally effectively using the optical fibre-based sensors.

II. WORKING PRINCIPLE OF FBG-BASED ACOUSTIC EMISSION MONITORING SYSTEM

FBGs are in-fibre sensing devices which can be ‘inscribed’ into a photosensitive optical fibre (as discussed earlier [19]), inducing a periodic change in the refractive index of the fibre core. Light is reflected at the Bragg wavelength, given by the effective refractive index of the fibre core, n_{eff} , and the periodic spacing of the grating, Λ ,

$$\lambda_B = 2 n_{eff} \Lambda \quad (1)$$

The change in the Bragg wavelength is calibrated as a function of a measurand (typically strain or temperature) applied to the small FBG. This wavelength shift can readily be using either an optical filter or a tunable laser [13] method. Thus the acoustic information required may be determined.

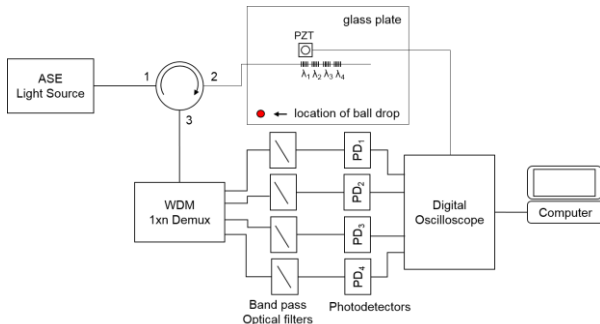


Fig. 1. A typical FBG-based cascaded acoustic sensor system, coupled with a PZT acoustic sensor, co-located with FBG₁, for cross-comparison.

Fig. 1 shows a schematic of the set-up used in this work, based on a cascaded FBG-based acoustic sensor system, coupled (with a PZT acoustic sensor for corss-comparison), co-located with sensor FBG₁. Light is emitted from a C-Band ASE light source into port 1 of an optical circulator, with a maximum output of 20.9 dBm. The signal reflected from the cascaded FBG sensors is passed from port 2 to port 3 where a demultiplexer is used to monitor each specific FBG encoded wavelength shift signal, detected by the photodiode array.

This configuration allows the capture of high-frequency acoustic signals from the FBG sensors at wavelengths λ_n (termed FBG_n, where $n = 1,2,3,4,\dots$) readily to be cross-compared with that received by the co-located PZT sensors.

III. ACOUSTIC SOURCE LOCALIZATION METHOD

In this work, a ball dropping simulated the AE signal and its location (as shown schematically in Fig.1), is determined using data received by the FBG-based sensor array and time-domain triangulation [30]. This familiar method allows high quality, high accuracy measurements in the real-time for this key challenge that marine structures are facing.

As illustrated in Fig.2, an array of three sensors is envisaged, and located respectively at points $S_0(0, 0)$, $S_1(x_1, y_1)$ and $S_2(x_2, y_2)$. The location of the acoustic emission source at $P(x, y)$ is thus defined as follows, assuming the distance between P and S_0 is r , as shown on the figure.

$$\delta_1 = PS_1 - PS_0 = \Delta t_{10} \cdot v \quad (2)$$

$$\delta_2 = PS_2 - PS_0 = \Delta t_{20} \cdot v \quad (3)$$

where, v is the velocity of acoustic wave propagation in the material (with the reasonable assumption that the material is uniform) and Δt_{10} and Δt_{20} respectively represent the arrival time differences of the signals received by sensors 1 and 0 and sensors 2 and 0 respectively.

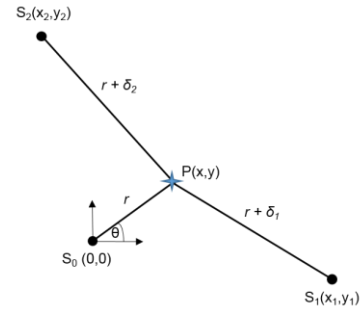


Fig. 2. Emission signals from Source P can be detected by an arbitrary 3-sensor array at different locations with different arrival times

$$x^2 + y^2 = r^2 \quad (4)$$

$$(x - x_1)^2 + (y - y_1)^2 = (r + \delta_1)^2 \quad (5)$$

$$(x - x_2)^2 + (y - y_2)^2 = (r + \delta_2)^2 \quad (6)$$

Using the trigonometric functions (4) - (6), the distance from the source and the ‘zero point’ can be calculated as:

$$r = \frac{A_1}{2 \cdot (x_1 \cdot \cos \theta + y_1 \cdot \sin \theta + \delta_1)} = \frac{A_2}{2 \cdot (x_2 \cdot \cos \theta + y_2 \cdot \sin \theta + \delta_2)} \quad (7)$$

where,

$$A_1 = x_1^2 + y_1^2 - \delta_1^2 \quad (8)$$

$$A_2 = x_2^2 + y_2^2 - \delta_2^2 \quad (9)$$

Equation (7) can be further expanded to,

$$(A_1 \cdot x_2 - A_2 \cdot x_1) \cdot \cos\theta + (A_1 \cdot y_2 - A_2 y_1) \cdot \sin\theta = \frac{A_2 \cdot \delta_1 - A_1 \cdot \delta_2}{\sqrt{(A_1 x_2 - A_2 x_1)^2 + (A_1 y_2 - A_2 y_1)^2}} \quad (10)$$

The final equation used for the calculation of the angle θ is given as Eq. (11).

$$\theta = \frac{(A_1 x_2 - A_2 x_1) \cdot \cos\theta}{\sqrt{(A_1 x_2 - A_2 x_1)^2 + (A_1 y_2 - A_2 y_1)^2}} + \frac{(A_1 y_2 - A_2 y_1) \sin\theta}{A_2 \delta_1 - A_1 \delta_2} = \frac{A_2 \delta_1 - A_1 \delta_2}{\sqrt{(A_1 x_2 - A_2 x_1)^2 + (A_1 y_2 - A_2 y_1)^2}} \quad (11)$$

The angle θ could thus be determined precisely from the known positions of the sensors S_1 and S_2 and measured signal time arrival differences at those points, corresponding to the position of S_0 , Δt_{10} and Δt_{20} and the known acoustic propagation velocity. Naturally, a value of θ yielding a positive value of r in Eq. (7) must be determined in order to have a valid solution. Knowing the absolute time of arrival and two time differences, the location of the excitation source can then be calculated.

IV. CALIBRATION – ACOUSTIC DETECTION USING GLASS PLATE

Calibration tests, using a glass plate as a sample onto which both optical and electrical sensors were bonded are shown schematically in Fig.1. Cyanoacrylate glue was specifically chosen (as it has worked well in prior research by the authors [27]) to ensure a ‘true’ transfer of the acoustically generated wave to the sensors integrated into the glass plate and the same arrival time of the acoustic signals using both sensors (in air in this case). Limited trials were successfully undertaken with a marine propeller [33] in water with the same glue and other FBG-based sensors, where the strain transfer was consistent, but this was carried out over only a short period of exposure – a few days. Exposure over a longer period, especially in sea water, would show any deleterious effects.

A tiny steel ball being dropped was used as a standardized excitation source and the glass plate was resting on 3 ball bearings (see Fig.1). To analyze the arrival times and shapes of the waveforms in the time domain, a set of typical data obtained from both FBG₁ and the co-located PZT sensor was recorded after a 0.2 g ball drop – this is plotted in Fig. 3.

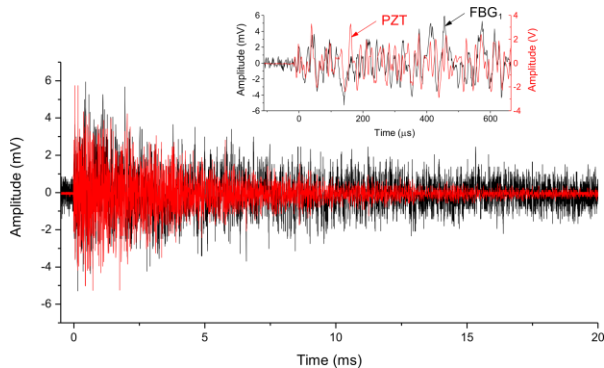


Fig. 3. Waveforms detected from both PZT and FBG₁ sensors after excitation of a tiny steel ball

As indicated in Fig.3 (inset diagram), the acoustic signals detected by both sensors are shown to have a close match, both

in terms of the arrival time and of the shape of the waveform. These findings demonstrate that meaningful AE data can be obtained using FBG-based acoustic sensors.

V. ACOUSTIC EMISSION DETECTION USING HALF-LIFTING SURFACE PLACED IN A WATER TANK

A. Experimental Setup

A key objective of this work is to show that the optical fibre-based techniques discussed can be applied in new ‘real world’ situations with confidence, and thus Fig. 4 shows the dimension and layout of the marine lifting body under investigation and instrumented with the sensors.

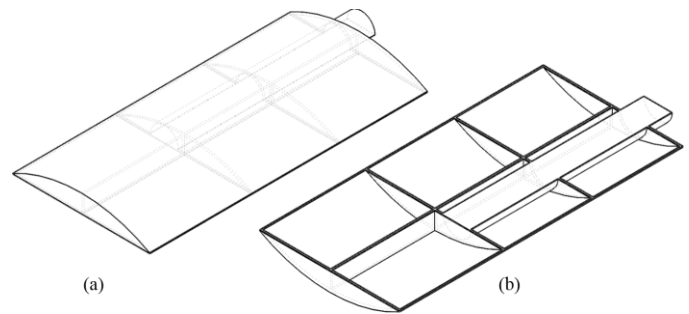


Fig. 4. Design of the marine lifting surface with the a) upper surface where the sensors are to be installed, b) inner surface with the shaft

All the sensors, including the 4 FBG-based acoustic sensors and the 4 co-located PZT acoustic sensors are instrumented onto the upper surface of this marine lifting structure, as illustrated in Fig.4 (a). The measurements are undertaken at a room temperature, mirroring the typically steady temperature of the local marine environment. However a correction for any temperature changes can readily be added – a further set of FBGs configured to be sensitive *only* to temperature is used, so that the acoustic signal only is determined [31-32].

Fig. 5 shows the overall sensor distribution and coordinates of the sensing points of interest. Both types of sensors were used to record the signal arrival times at these known sensor locations (marked as S_0 to S_3 in Fig 5).

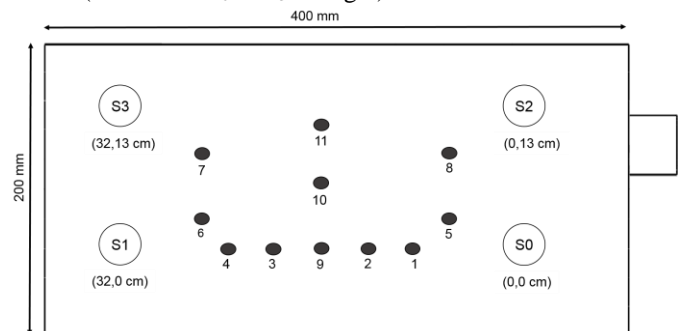


Fig. 5. Overall distribution of positions (dark dots) where the impact was applied during the tests. FBG-based acoustic sensors and PZT sensors locations are marked S_0 , S_1 , S_2 and S_3 .

The standardized acoustic impacts were applied using an ultrasonic sonotrode with a frequency of 26 kHz, at various locations. Fig. 5 shows 11 points where the excitation was applied sequentially – tests were repeated several times to show consistency. The points are represented by dark dots on Fig. 5

and their locations in the coordinate system are provided in Table 1. (The speed of sound used in this case is speed of sound of the steel and it is 5600 m/s). In the next stage of the evaluation, cavitation tests were carried out and Fig. 6 shows a set up for the test-rig used for such cavitation tests. A steel marine lifting surface, which is placed in a water tank with the excitation sonotrode mounted 1 mm above the upper surface. The sonotrode standard frequency used again is 26 kHz and the maximum power of 200W. The marine lifting surface was not fixed rigidly, but suspended (see Fig. 6).

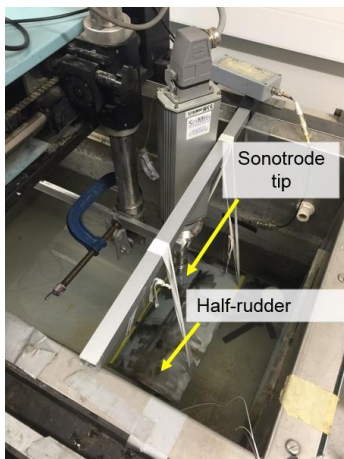


Fig. 6. Cavitation tests of the half-rudder instrumented with both FBG and PZT acoustic sensors

B. Experimental Results

The data collected from both types of sensor were analyzed in both the time and the frequency domains, where the latter is used to verify the excitation frequency. In the time domain, the time of arrival of the waveform detected by sensor array at known locations is used to determine the acoustic emission source location, through applying equations (7) and (11). All 11 impact points are excited several times to evaluate the repeatability of the measurements and to minimize experimental uncertainty.

1) Impact point in the middle of the lifting surface with coordinates (16, 7 cm)

Fig. 7 shows typical results – the waveforms recorded by both FBG₀ and the co-located PZT sensor when the excitation is located at point 10, as shown in Fig. 7. The data have shown exactly the same arrival time due to the same location.

Further work has enabled Fig. 8 to show the signals detected by FBG-based acoustic sensors at positions S₀, S₁, S₂ and S₃ for the same excitation point. The four waves are shown to arrive at a similar time, as expected, (as the source is placed in the middle of the marine lifting surface). The similar arrival time was first visually observed, and then verified by using a cross-correlation function applied to certain parts of the waveform – those where the signal was not affected by various reflections observed during the excitation. This similar arrival time, verified by the cross-correlation function, indicates that the signals detected at all the sensor positions, are matching in phase. S₀ and S₂ see the peak signal arriving slightly ahead of

that at S₁ and S₃, indicating a slight deviation of the excitation from the centre to the right of the test sample.

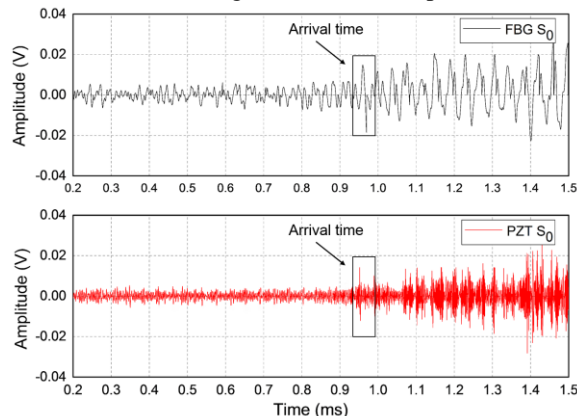


Fig. 7. Acoustic signals acquired by both FBG-based acoustic sensor and co-located conventional PZT sensor indicating similar time of arrival.

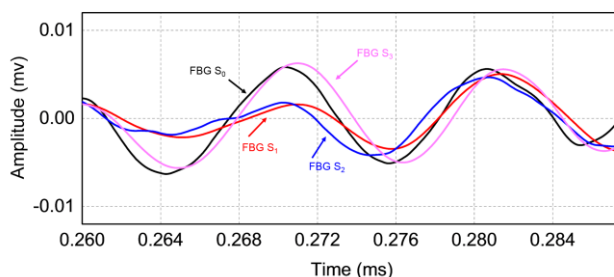


Fig. 8. Acoustic signals acquired by the optical based acoustic sensors at all four sensor locations of the half-rudder when rudder was subject to excitation of the sonotrode.

Fig. 9 shows the frequency-domain data obtained from all the FBG-based acoustic sensors used and the response from co-located PZT sensors. The data verify the known ‘standard frequency’ of the sonotrode excitation, of 26 kHz.

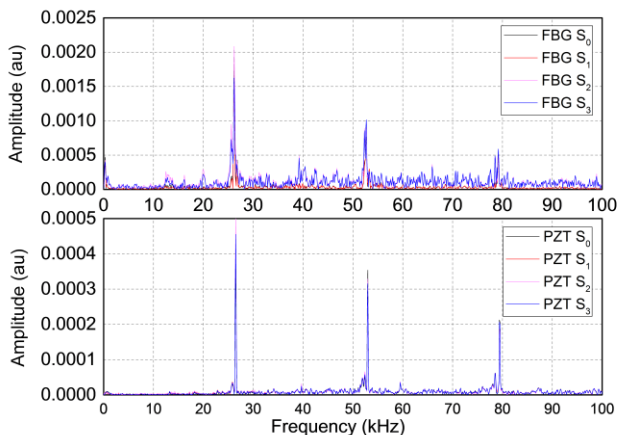


Fig. 9. Frequency response of FBG-based acoustic sensors and PZT acoustic sensors indicating a close match of standard sonotrode frequency of 26 kHz.

Fig.9 also shows that there is a close match in the frequency domain data from the data received from both types of sensors used, when the marine lifting surface was used under the sonotrode excitation.

2) Impact point between sensor locations S_0 and S_1 with coordinates (16, 0 cm)

Fig. 10 shows the waveforms recorded by both the FBG-based optical sensors and the co-located PZT sensors when the sonotrode excitation is placed above position 9, which is located between S_0 and S_1 on the figure. Again, both sensors have indicated the same arrival time for the signal.

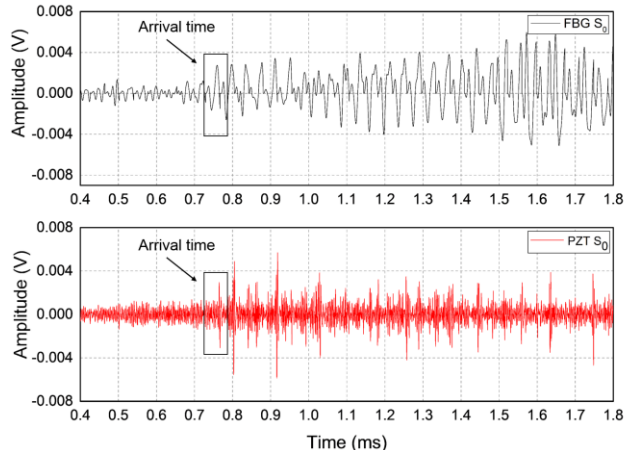


Fig. 10. Acoustic signals acquired by both FBG-based acoustic sensor and co-located conventional PZT sensor indicating similar time of arrival.

Figure 11 shows the data received by all the four sensors of each type (FBG and PZT) used. Sensors 1 and 0 positions received the signals the first as expected, due to their closer locations to the excitation compared to Sensors 2 and 3. Again the slightly early arrival of the signal at the position of Sensor 2 compared to Sensor 3 indicates that the excitation is slightly offset to the right: this is evident by the value of Δt_{10} (measured to be $0.88\mu\text{s}$ and rather than the expected zero (from the reference)) and thus having been based on the assumption that that source was located exactly in the middle of those two sensing points. This positional error was possibly caused by the movement of the rudder, while being excited.

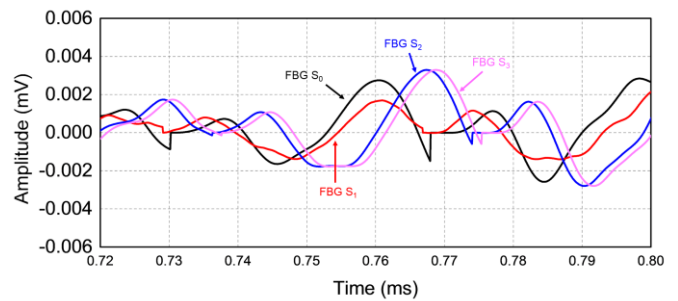


Fig. 11. Acoustic signals acquired by the optical based acoustic sensors at all four sensor locations of the marine lifting surface when it was subject to excitation of the sonotrode

Fig. 12 shows the frequency-domain data obtained from all FBG-based acoustic sensors and also from the PZT sensors when the sonotrode was mounted between the S_0 and S_1 sensor points. It is encouraging to see from these results that it is clearly indicating the standard frequency of the sonotrode used, which is 26 kHz.

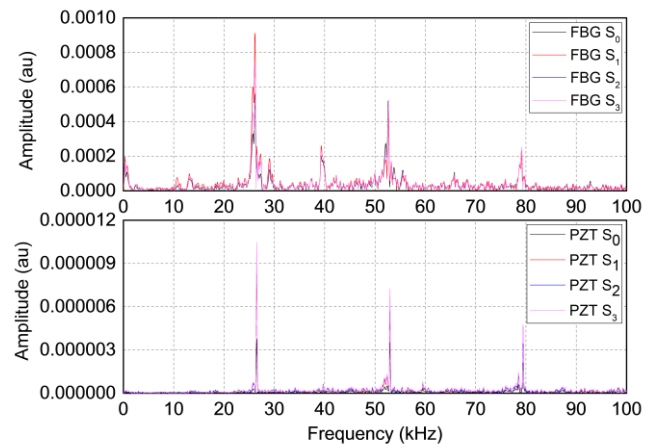


Fig. 12. Frequency response of FBG-based acoustic sensors and co-located PZT acoustic sensors indicating capture of standard sonotrode frequency

The data collected show that the frequency domain data captured by all four PZT acoustic sensors show a close match with the frequency-domain data captured by FBG-based acoustic sensors, giving confidence in the optical sensor technique. Considering the close match in results obtained, it shows that optical technique is well suited to this type of application.

C. Summary of the results obtained

The work has shown very clearly the quality of the data that may be obtained from the use of tailored fibre optic sensors and the excellence of the cross-comparison between their outputs and those from conventional PZT sensors widely used in industry. The data seen in Table I show a summary of the calculated locations obtained using equations (7) and (11) and the arrival times captured by both fibre optic and electrical sensors when the excitation is located at 11 different positions, as indicated in Fig.7. The small deviation in the estimation of the location could be caused by the small differences in the set up for the two sets of experiments carried out: thus the mobility of the marine lifting surface or the slightly different positioning of the excitation source can cause such deviations.

TABLE I
CROSS COMPARISON BETWEEN FBG AND PZT DETECTED SOURCE COORDINATES (X, Y)

Expected source coordinates [cm]	Source coordinates detected by FBGs [cm]	Source coordinates detected by PZTs [cm]
1 (10,0)	(11, 0.2)	(9.4, 0.28)
2 (13,0)	(13.4, 0.24)	(13, 0.12)
3 (19,0)	(19.7, 0.1)	(20.8, 0.35)
4 (22,0)	(23.1, 0.25)	(23, 0.24)
5 (8,3.2)	(9.2, 3.4)	(9, 3.1)
6 (24,3.2)	(24.2, 3.6)	(23.8, 3.4)
7 (24,9.8)	(26.4, 10.5)	(24.1, 9.6)
8 (8,9.8)	(7.4, 10.4)	(7.4, 10.1)
9 (16,0)	(15.2, 0.4)	(15.3, 0.25)
10 (16,7)	(16.8, 7.6)	(16.2, 7)
11 (16,14)	(16, 14.1)	(15.6, 14.3)

Fig. 13 shows in a simple illustration a cross comparison between the two sensor types used (the red circles represent the known sonotrode excitation points and the blue and black crosses, respectively represent the calculated locations of the excitation source based on the data obtained from the PZT and FBG sensors). The pattern of close agreement between the results obtained with the two sets of sensors is evident.

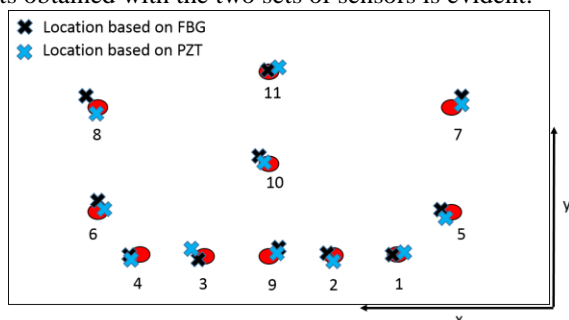


Fig. 13. Calculated acoustic emission source locations based on the data from both FBG-based acoustic sensor (represented by ‘x’) and PZT based acoustic sensor (represented by ‘x’)

The largest deviation seen between the calculated and the known locations is observed to be at location 7. This likely arises as it is a position which is quite close to the edge and thus the number of reflections at the edge of the rudder or the movement of the half-rudder in the water after excitation as the rudder not being fixed during the whole course of the tests could likely have caused this. The deviation between the point of impact (assumed the ‘true location’) and the point measured by the FBG-based and the PZT-based sensors is tabulated below in Table II, with the average deviation determined (assuming all deviations are ‘positive’). This again verifies that a high quality result can be seen from the use of the FBG-based sensors.

VI. CONCLUSIONS

A multipoint measurement fibre optic, FBG-based acoustic sensor system has been successfully developed and verified through both laboratory-based glass plate tests and

TABLE II
DEVIATIONS MEASURED USING BOTH FBG-BASED AND PZT-BASED SENSORS (X, Y)

Impact Point	Deviation Measured Using FBG-based sensor [cm]	Deviation Measured using FBG-based sensor [%]	Deviation Measured Using PZT-based sensor [cm]	Deviation Measured using PZT-based sensor [%]
1	(1, 0.2)	(10, 6.7)	(0.6, 0.28)	(6, 9.3)
2	(0.4, 0.24)	(3.1, 8)	(0, 0.12)	(0, 4)
3	(0.7, 0.1)	(3.7, 3.3)	(1.8, 0.35)	(9.5, 11.7)
4	(1.1, 0.25)	(5, 8.3)	(1, 0.24)	(4.5, 8)
5	(1.2, 0.2)	(15, 6.3)	(1, 0.1)	(12.5, 3.1)
6	(0.2, 0.4)	(0.8, 12.5)	(0.2, 0.2)	(0.8, 6.3)
7	(2.4, 0.7)	(10, 7.1)	(0.1, 0.2)	(0.4, 2.0)
8	(0.6, 0.6)	(7.5, 6.1)	(0.6, 0.3)	(7.5, 3.1)
9	(0.8, 0.4)	(5, 13.3)	(0.7, 0.25)	(4.4, 8.3)
10	(0.8, 0.6)	(5, 8.6)	(0.2, 0)	(1.3, 0)
11	(0, 0.1)	(0, 0.7)	(0.4, 0.3)	(2.5, 2.1)
Average Deviation	(0.854, 0.49)	(5.9, 7.4)	(0.61, 0.22)	(4.5, 5.3)

simulated cavitation tests on a marine lifting surface. Results show the acoustic source location has been successfully determined using the triangulation method and a very good

agreement between optical and PZT sensors reached. The small deviation seen between the results with the two methods can be attributed to small differences in the two experimental conditions, from factors such as the mobility of the lifting surface, movement of the sonotrode to give slightly different calculate results. The (known) excitation frequency of the sonotrode was determined with the optical method, within the uncertainty of the measurement. Their light weight, ease of multiplexing of the sensors and their immunity to EMI are the key benefits demonstrated for fibre optic sensors in this application. Future work will focus on scaling-up the instrumentation by integrating further sensor arrays into two model rudders, twice the size of the existing model, to explore more fully any scaling effects.

ACKNOWLEDGMENT

The authors wish to thank you to BAE Systems for providing the sample of the marine lifting surface for extensive testing and Assent Engineering Ltd for providing the PZT acoustic sensors used in this work.

REFERENCES

- [1] Carpinteri, A.; Lacidogna, G.; Pugno, N. Structural damage diagnosis and life-time assessment by acoustic emission monitoring. *Eng. Fract. Mech.* 2007, 74, 273–289.
- [2] Tan, A.C.C.; Kaphle, M.; Thambiratnam, D. Structural Health Monitoring of Bridges Using Acoustic Emission Technology. In *Proceedings of 8th International Conference on the Reliability, Maintainability and Safety, 2009 (ICRMS 2009)*, Chengdu, China, 20–24 July 2009; pp. 839–843.
- [3] Hee-Baek, Lee. Chung-Seo, Park. Seong-Mo, Son. Kyung-Jin, Park. Sang-Sik, Park. ”Combating Rudder Erosion with Cavitation-Resistant Coating”, *Journal of Protective Coatings and Linings*, vol. 32 no. 3, pp 38–41, (2000).
- [4] Daewon, Seo., Seung-Hee, Lee., Sang-Hyun, Kim., Jungkeun, Oh., ”Practically applicable devices for blocking the gap flow of a horn rudder to reduce rudder cavitation and their verification through numerical simulations”, *Journal of Marine Science and Technology*, vol. 17, no. 1, pp 18-29 (2011).
- [5] Carlton John, *Marine Propellers*, 3rd Edition, Butterworth-Heinemam, 2012.
- [6] T. He., Q. Pan., Y. Liu., X. Liu., D. Hu., “Near-field beamforming analysis for acoustic emission source localization”, *Ultrasonics*, vol. 52 (5), pp. 587-592 (2012).
- [7] J L., Rose., “*Ultrasonic Waves in Solid Media*“, Cambridge University Press, Cambridge (1999).
- [8] D, Roy, Mahapatra., S, Gopalakrishnan., “A spectral finite element model for analysis of axial-flexural shear coupled wave propagation in laminated composite beams“, *Composite Structures*, vol. 59, pp. 67-88, (2002).
- [9] S, Gopalakrishnan., A, Chakraborty., D, Roy, Mahapatra., “*Spectral Finite Element Method: Wave Propagation, Diagnostics and Control in Anisotropic and Inhomogeneous Structures*“, Springer, Berlin, (2007).

- [10] Nair, A., Cai, C., "Acoustic Emission monitoring of bridges: Review and case studies" *Engineering Structures*, vol. 32, pp 1704-1714 (2010).
- [11] Kageyama, K., Murayama, H., Ohsawa, I., Kanai, M., Nagata, K., Machijima, Y., Matsumara, F., "Acoustic emission monitoring of a reinforced concrete structure by applying a new fibre-optic sensors", *Smart Materials Structure*, vol. 14, pp. S52-S59 (2005).
- [12] Qin, Y, Liang, Z, Zhang, Y., Zhang, G., "Experimental Study on an Optical Fiber Acoustic Emission Array". In proceedings of Laser Physics and Laser Technologies, Harbin, China, pp 299-302 (2010).
- [13] Liang, Y., Mu, L., Liu, J., Yu, X., "Combined optical fiber interferometric sensors for the detection of acoustic emission". *Optoelectron Letter*, vol. 4, pp. 184-187, (2008).
- [14] Masturo, T., Cho, H., Takemoto, M., "Optical fiber acoustic emission system for monitoring molten salt attack". *Sci. Technol. Adv. Mater.*, vol. 7, pp. 104-110, (2006).
- [15] Liang, S., Zhang, C., Lin, W., Li, L., Li, C., Feng, X., "Fiber Optic intrinsic distributed acoustic emission sensor for large structure health monitoring". *Optical Letter*, vol. 34, pp 185-1860, (2009).
- [16] Tsuda, H., Takahashi, J., Urabe, K., Ikeguchi, T., "Damage monitoring of carbon fiber-reinforced plastic with Michelson interferometric fibre-optic sensors". *J. Material Science*, vol. 34, pp. 4163-4172, (1999).
- [17] Tsuda, S., Okabe, Y., Yamamoto, T., Takeda, N., "Detection of edge delamination in CFRP laminates under cyclic loading using small-diameter FBG sensors". *Compos. Sci. Technol.*, vol. 63, pp. 1885-1894, (2003).
- [18] Hill, D.J., "DFB fibre-laser sensor developments" *Proceeding Spie*, vol. 5855, pp. 904-907, (2005).
- [19] Huang, W., Ma, H., Zhang, W., Li, F., Liang, Y., "Rock mass acoustic emission detection using DFB fiber lasers". *Proceeding Spie*, (2012).
- [20] Grattan, K. T. V. and Sun, T., "Fiber optic sensor technology: An overview", *Sens. Actuators A: Phys.*, vol. 82, no. 1-3, pp. 40-61, (2000).
- [21] Tsuda, H., Sato, E. Nakajima, T. and Sato, A., "Development of fibre optic broadband vibration-detection system," *Synthesiology* 6(1), 45-54 (2013)..
- [22] Kersey, A., Davis, M., Patrick, H., et al. "Fiber grating sensors", *Journal of Lightwave Technology* 15(8): 1442-1463, (1997).
- [23] Wild, G. and Hinckley, S., "Acousto-ultrasonic optical fiber sensors: Overview and state-of-the-art", *IEEE Sensors Journal*, vol. 8, pp. 1184-1193 (2008).
- [24] Tsuda, H., Kumakura, K. and Ogihara S, "Ultrasonic sensitivity of strain-insensitive fiber Bragg grating sensors and evaluation of ultrasound-induced strain", *Sensors* 10: 11248-11258, (2010). "Synthetic structure of industrial plastics," in *Plastics*, 2nd ed., vol. 3, J. Peters, Ed. New York: McGraw-Hill, 1964, pp. 15-64.
- [25] Perez, I., Cui, HL. and Udd, E., "Acoustic emission detection using fiber Bragg gratings", *Proceedings of SPIE 4328 Smart Structures and Materials 2001: Sensory Phenomena and Measurement Instrumentation for Smart Structures and Materials*: 209-215, (2001).
- [26] Wild, G. and Hinckley, S., "Optical Fibre Bragg Gratings for Acoustic Sensors," *Proc. 20th Int. Congress on Acoustics* (2010).
- [27] Grattan, K. T. V. and Meggitt, B. T., [Optical Fiber Sensor Technology: Fundamentals], Kluwer Academic Publishers, London, ISBN 0 79237852 0, (2000).
- [28] Ioannis Armakolas, John Carlton, Miodrag Vidakovic, Tong Sun, K.T.V. Grattan, "The acoustic signatures of cavitation erosion on grade DH36 steel", *Journal of Physics Conference Series* 656 (1), December 2015.
- [29] Anastasopoulos, A., Kourousis, D., Botten, S. and Wang, G. (2009), "Acoustic emission monitoring for detecting structural defects in vessels and offshore structures", *Ships and Offshore Structures*, vol.4, pp. 363-372
- [30] A, Tobias., "Acoustic-emission source location in two dimensions by an array of three sensors", *Non-Destructive Testing*, (1976).
- [31] Sun, T., Grattan, K. T. V., Srinivasan, S., Basheer, P.A.M., Smith, B. J. & Viles, H. A. (2012). *Building Stone Condition Monitoring Using Specially Designed Compensated Optical Fiber Humidity Sensors*. *IEEE Sensors Journal*, 12(5), pp. 1011-1017.
- [32] Mokhtar, M., R., Owens, K., Kwasny, J., Taylor, S. E., Basheer, P. A. M., Cleland, D., Bai, Y., Sonebi, M., Davis, G., Gupta, A., Hogg, I., Bell, B., Doherty, W., McKeague, S., Moore, D., Greeves, K., Sun, T., Grattan, K. T. V. Fibre - optic strain sensor system with temperature compensation for arch bridge condition monitoring. *IEEE Sensors Journal*, 2012, vol.12, issue 5,
- [33] Javdani, S., Fabian, M., Carlton, J., Sun, T. & Grattan, K. T. V. (2016). Underwater free-vibration analysis of full-scale marine propeller using a Fibre Bragg Grating-based sensor system. *IEEE Sensors Journal*, 16(4), pp. 946-953.